Scattering by an anisotropic infinite cylinder: a modal approach

Nicolas Kossowski, Parry Yu Chen, Qi Jie Wang, Patrice Genevet, Yonatan Sivan

Scattering by an anisotropic infinite cylinder: a modal approach

Nicolas Kossowski[1], Parry Yu Chen[2], Qi Jie Wang[1], Patrice Genevet[3], and Yonatan Sivan[2]

[1]School of Electronic and Electrical Engineering, CINTRA, Nanyang Technological University, Singapore
[2]School of Electrical and Computer Engineering, Ben-Gurion University, Israel
[3]CNRS-Centre de Recherche sur l'Hetero-Epitaxie et ses Applications, Universite Cote d'Azur, France

August 12, 2020

Abstract

Scattering of anisotropic nanostructures has always been a challenging problem due to the complexity of the boundary conditions with the tensorial form of the permittivity, which is becoming even more challenging for non-conventional geometries. To solve these problems, it is necessary to consider strong hypothesis of lossless material and generic nanoparticle geometries, and only few solutions have achieved modal decomposition of interest to build physical intuitions. Here, we present an extension of the generalized normal mode expansion, applicable to scatterers with complex geometries composed of lossy and anisotropic materials. We illustrate our method by considering an infinitely long cylinder with concentric metallic/dielectric layers, targeting the complex case of hyperbolic metamaterial response, and identifying regimes of interest for applications, including back-scattering cancellation effect.

1 Introduction

Recent developments of metamaterials and metasurfaces bring the necessity to develop new tools to predict the scattering properties of new type subwavelength resonators. Some of these materials are anisotropic, essentially due to their inherent material composition or, by design for most of the metamaterials made of complex heterogeneous layers. The challenging problem of the scattering by anisotropic cylinders has been investigated, on one hand providing exact solutions with modal expansion for some specific cases such as for gyrotropic materials with fix circular geometries [1], and on the other hand, for other types of anisotropy for which the inherent complexity of the problem imposes the use of numerical solutions. Graglia and al. developed a integro-differential solution for arbitrarily shaped, lossy material [2, 3]. Monzon and al. introduced an integral solution for circular cylinders under normal [4] and oblique incidence [5]. Since

then, other methods have followed with variational approach [6], surface integrals [7, 8], method of moments [3], Fourier domain [9] and coupled-dipole approximation [10]. Recently, finite differences time-domain (FDTD) [11] and finite element method [12] are commonly used with software to extract the optical properties of complex nanostructures. However, direct simulations do not provide sufficient physical description in terms of the nanoparticle's eigenmodes. An analytical decomposition working for non-lossy materials with circular section can address this issue, expanding the eigenmodes on cylindrical wave functions [13], [14].

Finding an eigen-expansion for the most general case of arbitrarily shaped, lossy and anisotropic cylinders in open-systems, has not yet been demonstrated because the set of eigenmodes is no longer finite and do not follow usual orthogonal relationship. Leaky modes have to be introduced to describe the radiating loss of the system to the background [15]. These modes, also called quasi-normal modes or resonant states [16], are characterized by a complex eigenfrequency where the imaginary part represents the lifetime of the mode. They have been widely used in many domains of the physics to describe scattering problems. In the case of open-systems, they suffer from divergent field at infinity making the modal expansion valid only inside the inclusion unless additive terms have to be taken into account [17]. This approach has been used to study the scattering by bianisotropic, chiral or magnetic cylinders [18].

Alternatively, the properties of the material could be considered as the eigenvalue of the problem. Taking the permittivity as a step function of all space combined with the use of the Lippman equation, is used to generate a complete orthogonal set of modes solution of a symmetrical operator for which the permittivity is the eigenvalue [19]. Another approach would be to define a linear integro-differential operator the conductivity is the eigenvalue giving a modal decomposition of the electric current density [20].

In this paper, we adapted the generalized normal mode expansion (GENOME) [19] to the case of anisotropic materials and validate our method using Mie theory. The applicability of our method is then exploited to analyse the particular scattering case of an infinite hyperbolic metamaterial cylinders with concentric metal/dielectric layers. Considering the coherent superposition of the scattered mode reveals new physical insight on the radiation properties of such structures, and in particular the observation of Kerker conditions in hyperbolic regime.

2 Generalized Normal Modes Expansion

We consider a cylinder with anisotropic material of permittivity $\bar{\bar{\epsilon}}_i$ embedded in a isotropic medium ϵ_b illuminated by an incident wave $\boldsymbol{E}_0$. The contrast between the permittivity $\Delta\bar{\bar{\epsilon}}$ between the two media induces a depolarizing current density, $\boldsymbol{J}_s(\boldsymbol{r}) = k^2\theta(\boldsymbol{r})\Delta\bar{\bar{\epsilon}}\boldsymbol{E}(\boldsymbol{r})$ where $\theta(\boldsymbol{r})$ is a step function imprinting the geometry of inclusion. This secondary source of current $\boldsymbol{J}_s(\boldsymbol{r})$ generate an electric field $\boldsymbol{E}_s(\boldsymbol{r})$ given by the Green's function $\bar{\bar{G}}_0(\boldsymbol{r},\boldsymbol{r}')$ by $\boldsymbol{E}_s(\boldsymbol{r}) = \int \bar{\bar{G}}_0(\boldsymbol{r},\boldsymbol{r}')\boldsymbol{J}_s(\boldsymbol{r}')d\boldsymbol{r}'$. With operator notation, we can rewrite the scattered field as $|E_s\rangle = \hat{\Gamma}\hat{C}\,|E\rangle$ where $\hat{\Gamma}\hat{C}$ is a linear integral operator. In our notation, $\hat{\Gamma}$ indicates the integral operator on the surface of the inclusion and $\hat{C}$ is to emphasize the presence of the tensor of permittivity contrast $\Delta\bar{\bar{\epsilon}}$

{eq:op}
$$\hat{\Gamma}\hat{C}\,|E\rangle = k^2 \int \theta(\boldsymbol{r}')\bar{\bar{G}}_0(\boldsymbol{r},\boldsymbol{r}')\Delta\bar{\bar{\epsilon}}\boldsymbol{E}(\boldsymbol{r}')d\boldsymbol{r}'. \tag{1}$$

In the case of isotropic materials [19], the operator (1) is symmetric since $\bar{\bar{G}}_0$ and $\Delta\epsilon\bar{\bar{I}}$ can commute, so the modes $\boldsymbol{E}_m$, also called basis modes, given by $s_m\,|E_m\rangle = \hat{\Gamma}\hat{C}\,|E_m\rangle$ define a complete orthonormal base of modes for the usual inner product $\langle E_m|E_n\rangle = \int \theta(\boldsymbol{r})E_m^\dagger(\boldsymbol{r})\cdot E_n(\boldsymbol{r})d\boldsymbol{r}$. For anisotropic material, the Green's function $\bar{\bar{G}}_0(\boldsymbol{r},\boldsymbol{r}')$ do not commute, in general, with the permittivity contrast $\Delta\bar{\bar{\epsilon}}$ making the operator (1) non-symmetric. Consequently, its modes do not form an orthogonal base of modes for the usual inner product. In other words, the complexity introduced the anisotropy resides in finding another inner product so that the modes are orthogonal. Such inner product is found by symmetrizing the operator (1), cf Appendix A and is defined by $\langle\tilde{E}_\mu|\hat{C}|\tilde{E}_\nu\rangle = \int \theta(\boldsymbol{r})\tilde{E}_\mu^\dagger(\boldsymbol{r})\cdot\Delta\bar{\bar{\epsilon}}\tilde{E}_\nu(\boldsymbol{r})d\boldsymbol{r}$. So, the modes $\tilde{\boldsymbol{E}}_\mu$, also called target modes and satisfying $\tilde{s}_\mu\,|\tilde{E}_\mu\rangle = \hat{\Gamma}\hat{C}\,|\tilde{E}_\mu\rangle$, form a complete set of orthogonal modes for the new inner product. It results that the total electric over all region of space is given by

{eq:etot}
$$|E\rangle \quad = \quad |E_0\rangle + \sum_\mu |\tilde{E}_\mu\rangle\,\frac{\tilde{s}_\mu}{1-\tilde{s}_\mu}\,\langle\tilde{E}_\mu|\hat{C}|E_0\rangle\,. \tag{2}$$

However, finding the target modes by solving the integral (or differential) equation they satisfy remains a challenging task. To overcome this issue, we re-expand the target modes in terms of modes of the isotropic inclusion [21]. Indeed, for simple geometries (e.g., a slab, cylinder, sphere), a set of orthogonal modes and their associated adjoints can be constructed by using the preknowledge of the functional form of the eigenmodes [22, 23, 24, 25, 19] and employing an efficient complex root search [26]. In more complicated geometries, one can always resort to a numerical approach [19, 27]. Clusters of scatterers can be treated with minimal overhead computations by the rigorous hybridization approach described in [28, 29, 20]. Writing $\tilde{\boldsymbol{E}}_\mu(\boldsymbol{r}) = \sum_m c_{\mu,m}\boldsymbol{E}_m(\boldsymbol{r})$, with $c_{\mu,m}$ the coefficient of the decomposition given by

{eq:sv}
$$\tilde{s}_\mu \boldsymbol{c}_\mu \quad = \quad \bar{\bar{S}}\,\bar{\bar{V}}\boldsymbol{c}_\mu, \tag{3}$$

where $\bar{\bar{V}}$ is the matrix of overlap integral between the modes of the isotropic inclusion, $\langle E_m|\hat{C}|E_n\rangle$, and $\bar{\bar{S}}$ is the diagonal matrix of eigenvalue s_m of the modes of the isotropic inclusion. Eq. (3) is key to understand how the modes of an anisotropic inclusion differ from the modes of an isotropic inclusion. One can easily verify that in the case of an isotropic inclusion, the overlap matrix is diagonal due to the absence of coupling between the modes. Eq. (3) then reduces to $\tilde{s}_\mu\boldsymbol{c}_\mu = \frac{\Delta\epsilon}{\epsilon_b}\,\mathrm{diag}[s_m]\boldsymbol{c}_\mu$ which is trivially solved by $\tilde{s}_\mu = \frac{\epsilon_i-\epsilon_b}{\epsilon_b}s_\mu$ and unitary vectors $\boldsymbol{c}_\mu$ (i.e. the

new base of modes is identical to the previous one, $\tilde{\boldsymbol{E}}_\mu = \boldsymbol{E}_\mu$). On the other hand, for anisotropic materials, the matrix of overlap integrals may not be diagonal. The presence of off-diagonal terms in the permittivity tensor induces mixing between modes that would be symmetry forbidden in the isotropic case. In fact, the target modes correspond to basis modes corrected by taking into account the coupling between the modes that is enabled by the anisotropy. It results also that the target modes, expressed as a complex superposition of modes of the isotropic inclusion, may not be explicitly identifiable by some intrinsic properties such as azimuthal orders or radial orders, as it is for the basis modes. Consequently, it may be more appropriate to rewrite Eq. (2) in terms of modes of the isotropic inclusion for practical applications, and so Eq. (2) becomes

{eq:Etot}
$$|E\rangle \quad = \quad |E_0\rangle + \sum_m \gamma_m \, |E_m\rangle \, . \tag{4}$$

where $\gamma_m = \sum_\mu c_{\mu,m} \frac{\tilde{s}_\mu}{1-\tilde{s}_\mu} \, \langle \tilde{E}_\mu | \hat{C} | E_0 \rangle$.

3 Numerical simulations of hyperbolic anisotropic infinite cylinder

In order to illustrate our re-expansion method for an anisotropic inclusion, we consider an infinite cylinder exhibiting hyperbolic behavior. Hyperbolic metamaterials are characterized by complex permittivity tensors and are studied for their unusual properties. Patterning and nanostructuring these materials is of great interest to realize new type of optical functions. Some structures have already been demonstrated with hyperbolic metamaterials such as tuning of absorption and scattering properties [30], indefinite cavities [31, 32], wavefront manipulation [33], enhancement of spontaneous emission [34], high temperature epsilon-near-zero emitters [35]. Recently, few works has been done on layered cylinders which have an effective hyperbolic optical response that show superscattering effect [36] or invisibility [37].

The dispersion relationship in such material is given by

{eq:disphmm}
$$\frac{k_{\phi,z}^2}{\epsilon_\rho} + \frac{k_\rho^2}{\epsilon_{\phi,z}} = k_0^2, \tag{5}$$

where $k_{\phi,z}$ and k_ρ are the in-plane and out-of-plane components of the wavevector in the cylinder and the sign of the real part of the in-plane and out-of-plane components of the permittivity tensor have opposite signs, $\mathrm{Re}(\epsilon_{\phi,z})\,\mathrm{Re}(\epsilon_\rho) < 0$. The domain where $\mathrm{Re}(\epsilon_{\phi,z}) > 0$ is called type I and the domain where $\mathrm{Re}(\epsilon_{\phi,z}) < 0$ is called type II [38, 39].

In what follows, we shall consider an infinite cylinder with circular cross-section (Fig. 1 (a)) of radius $R = 90\ nm$. The cylindrical inclusion consists of concentric multilayers of silver [40] and titanium oxide [41] known to present hyperbolic behaviour in the visible [42]. We denote, p the filling factor of silver in the composite. We assume that the layers are thin enough so that we can apply the effective medium theory [43], resulting in a homogeneous uniaxial anisotropic in the cylindrical coordinate system,

{eq:diel}
$$\bar{\bar{\epsilon}} = \begin{pmatrix} \epsilon_\rho & 0 & 0 \\ 0 & \epsilon_{\phi,z} & 0 \\ 0 & 0 & \epsilon_{\phi,z} \end{pmatrix}_{(\hat{\boldsymbol{e}}_\rho, \hat{\boldsymbol{e}}_\phi, \hat{\boldsymbol{e}}_z)} , \tag{6}$$

where

{eq:epsilon}
$$\epsilon_{\phi,z} = p\epsilon_{Ag} + (1-p)\epsilon_{TiO_2}, \qquad \epsilon_\rho = \frac{1}{\frac{p}{\epsilon_{Ag}} + \frac{1-p}{\epsilon_{TiO_2}}}, \tag{7}$$

Here, we emphasize that we do not consider the material as lossless and so, the permittivities of the titanium oxide, ϵ_{TiO_2}, and silver ϵ_{Ag} are complex. We note also that the tensor is diagonal and therefore satisfy condition on the material so that we can apply GENOME. Besides, there is a singularity at the center of the cylinder since the permittivity tensor is defined in a cylindrical base and therefore the permittivity is not defined at the origin.

The source is a plane wave propagating along the $x-$direction with an in-plane polarization. The basis of modes of the equivalent isotropic structures is determined with exact calculation for the transverse modes [44] and the longitudinal modes [21]. The details of the derivation of overlap integrals between the modes, Eq. (32), and the incident fields, $\langle \tilde{E}_\mu | \hat{C} | E_0 \rangle$ are presented in Appendix D and Appendix E.

3.1 Validating the re-expansion approach with COMSOL

To validate our model, we have compared the electric field generated by Eq. (44) with the solution given by Mie theory [45, 46]. We computed Mie solution with 100 modes. The relative error between the Mie solution and our GENOME computation, Eq. (44), is evaluated by using the L_2-norm,

{eq:error}
$$\Delta\eta_R = \frac{\left\|\mathrm{Re}(\boldsymbol{E}_{mie} - \boldsymbol{E}_{gen})\right\|_2}{\|\mathrm{Re}(\boldsymbol{E}_{mie})\|_2}, \tag{8}$$

$$\Delta\eta_I = \frac{\left\|\mathrm{Im}(\boldsymbol{E}_{mie} - \boldsymbol{E}_{gen})\right\|_2}{\|\mathrm{Im}(\boldsymbol{E}_{mie})\|_2}. \tag{9}$$

For this test, we consider the operating wavelength of 470 nm and $p = 0.7$. We performed the calculation initially with 1360 transverse modes, azimuthal orders ranging from -8 to 8 and 80 radial orders, and 1700 longitudinal modes with azimuthal orders ranging from -8 to 8 and 100 radial orders. Then, we re-compute the solution more efficiently with only the most important modes that have been ordered by order of magnitude where at each iteration, we add modes couples with opposite azimuthal orders. Special attention as to be made in the resolution of Eq. (3). An accurate resolution of this equation is important since it conditions the decomposition of the target modes. However, due to the large amount of modes and due to the fact that most of the modes do not interact one with another, the matrix of the overlap integral $\bar{\bar{V}}$ can be ill-conditionned. In our case, since the permittivity tensor (6) is diagonal, there is no mode mixing between modes of different azimuthal orders, cf. Appendix D. So, we can re-arrange the matrix of overlap integral to be be block diagonal and resolve Eq. (3) for each azimuthal order independently. The size of each block is then determined by the number of radial orders that are considered.

The convergence plot between Mie and our solutions is shown in Fig. 1 (b). Outside the cylinder, we have respectable agreement between the two solutions, up to -35 dB. However, inside the cylinder the convergence reaches only -16 dB. The difference can be observed in the fields plot where at the center of the cylinder, closer to the singularity, the difference is the largest. The hard limit obtained in the convergence plot, results from missing high radial order longitudinal modes as shown in the mapping of the coefficient γ_n, Fig. 1 (d). The decrease of the magnitude

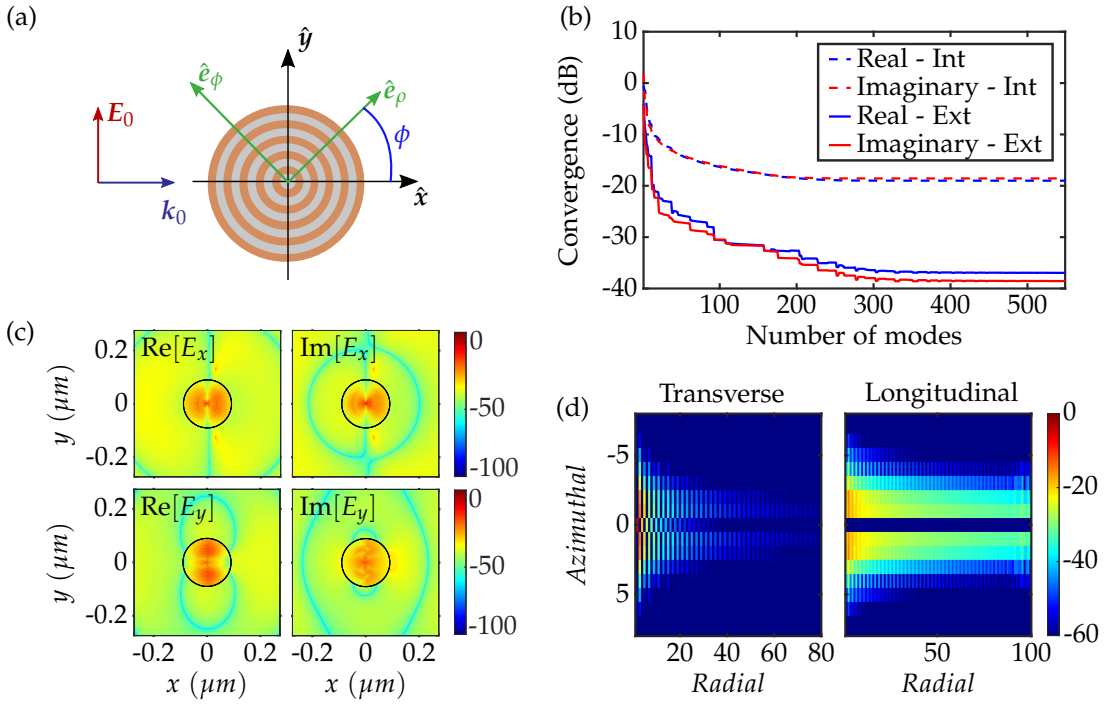

FIGURE 1: *(a) Schematic of the concentric layered scatterer. A linearly-polarized, transverse magnetic, incident plane wave propagates along the* $\hat{\mathbf{x}}$*. (b) Convergence between of the total electric field from Mie and GENOME solutions. The dashed line represents the convergence inside the cylinder and the plain line the convergence outside. (c) Difference, in* dB*, between the electric field computed with Mie and GENOME solutions. (d) Mapping of the coefficient* $|\gamma_n|$ *normalized by the highest coefficient, in* dB*. At* 470 nm*, the permittivities contrasts are* $\epsilon_\rho = 28.9272 + 5.7214i$ *and* $\epsilon_{\phi,z} = 1.2263 + 0.2779i$*.*

{fig:conv}

of the coefficient γ_n along the radial direction is slower for the longitudinal modes than for the transverse modes and so by considering up to 100 radial order for the longitudinal modes we can only achieve up to -15 dB accuracy. This behaviour results of the presence of the singularity at the center of the cylinder. The permittivity being undefined at this point, the electric field tends to infinity which is expressed by the superposition of the longitudinal modes. So, a large number of modes with high radial orders are required and it can be seen in Fig. 1 (c) with the red concentric rings.

3.2 Application to hyperbolic metamaterials

Using GENOME, we calculated the scattered field of the cylinder with diameter 180 nm for different composition of silver (p) in the composite.

For purely silver isotropic material, Fig. 2 $p = 1$, we observe the standard Mie resonances. Only transverse magnetic modes are excited, which is normal due to the polarization and incidence angle of the incident wave and the absence of coupling component in the permittivity tensor. The subscript *diel* and *plas* indicate the nature of the mode and is determined depending on the sign of the real part of the eigenpermittivity. Dielectric modes are associated with magnetic poles with $\mathrm{Re}(\epsilon_m) > 0$ whereas plasmonic modes are associated with electric poles with $\mathrm{Re}\,\epsilon_m < 0$. The number associated with the notation, indicates the rotational symmetry of the mode, so $T^H_{diel} : 0$ and $T^H_{diel} : \pm 1$ are magnetic dipoles whereas $T^H_{plas} : \pm 1$ is an electric dipole. As expected, for the purely silver, $p = 1$, the modes are dominated by strong electrical resonances. The magnetic resonances are relatively weak. In the case of a cylinder purely dielectric, $p = 0$, strong magnetic dipoles can be observed [47], as seen by the resonances of the dielectric modes. Besides, due to the relatively small radius, the electric dipolar resonances is non-negligeable. Now, looking at the modal decomposition of the scattered field for a composition $p = 0.4$ silver, Fig. 3. For the sake of the clarity, we plotted only the first few important modes. Concerning the scattering, we can observe several new peaks that do not correspond to the excitation of new modes but it corresponds to secondary and third resonances of the same modes. This can be interpreted as a "compression" of the spectrum since the effective refractive index increases due to the hyperbolicity of the material. Besides, in type I domain, the dielectric modes have an important role in the decomposition due to the sign of the tangential component of the permittivity tensor, $\epsilon_{\phi,z} > 0$, allows the circulation of free electron in the tangential direction. Conversely, in the type II domain, the metallic behavior in the tangential direction reduces those circulation current. So, it is coherent to observe the relatively effect low of the magnetic modes, such as in the case of a purely metallic material, and therefore the dominant electric dipole behavior. In terms of absorption, we can observe also two new absorption peaks. However, in this case, it corresponds to the resonance of the longitudinal components of the fields that are excited due to the anisotropy of the material. Overall, we note that the scattering efficiency decreases compared to the isotropic case, but this is explained by the relative increase of losses. Besides, we can observe a slight shift in the absorption and scattering peaks compare to the isotropic case. Taking into account the third and second resonances, it means we can further control the spectral position of scattering and absorption by tuning the geometrical and material property of the cylinder as in ref. [30]. But, tuning those properties allows also to control the scattering diagram of the nanostructure. As show, in the type I domain, where magnetic and electric modes co-exist with the same strength, it is possible to realize Kerker effect [48] as in Fig. 4 where the constructive and destructive interference of the excited modes results in the suppression of the back-scattering. The special case where the

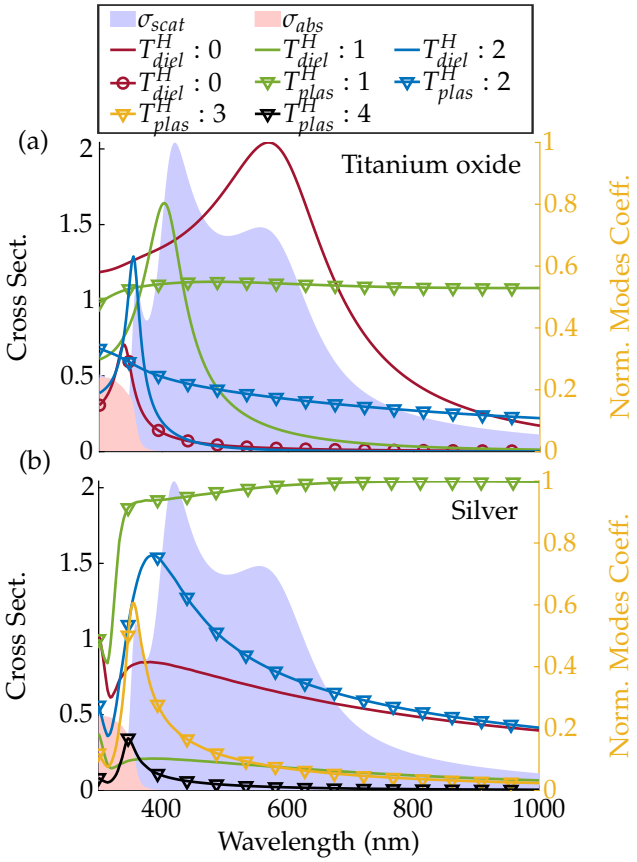

FIGURE 2: *Cylinder with diameter* 180 *nm for isotropic materials (a) Titanium oxide and (b) silver. The blue and red areas represent the scattering and absorption cross-sections, respectively, and are associated with the left y-axis. The cross sections have been normalized by the diameter of the cylinder. The curves represent the coefficient* $|\gamma_n|$ *for the most important modes. The coefficient have been normalized by the maximum of the most important modes.*

{fig:scatiso}

side lobes are also suppressed corresponds to the case where four modes superposed, an electric dipole, an electric quadrupole, a magnetic dipole and a magnetic quadrupole [49]. And our modal decomposition show that those four components are present and play an important role in the expression of the scattered field. Here, we emphasize that the scattered field do not result only from the superposition of these four modes but also from the residual modes that are not plotted. In this our modal decomposition differ from a multipolar analysis [50]. We also understand that such effect cannot be realized in the type II domain due to the absence of strong magnetic modes.

4 Outlook

In this paper, we presented an extension to the anisotropic materials of the generalized normal mode expansion. We solved the issue induced by the anisotropy by re-expanding the electric fields in terms of known solutions. We illustrated our method by comparing it with available commercial software and achieved reasonable agreement. The power of our tool relies in its capacity to solve the case of lossy materials and give comprehensive decomposition of the scattered field. We applied this tool to study the case of a scattering by a cylinder with hyperbolic concentric layers where we show how it can be used to interpret its scattering properties such as the absorption process and the cancellation of back-scattering in type I hyperbolic medium. Despite not being applicable to all anisotropic material, it can already be used to a subsequent number of scattering problems involving metamaterials such as heterostructures or hyperbolic metamaterials. In the specific case of circular cross-section cylindrical scatterers, the study can be extended to the case of oblique incidence, localized source in the near field. Finally, GENOME extended to anisotropic media paves the way for the exploration of properties of metamaterials for scattering problems, field enhancement or enhancement of spontaneous emission.

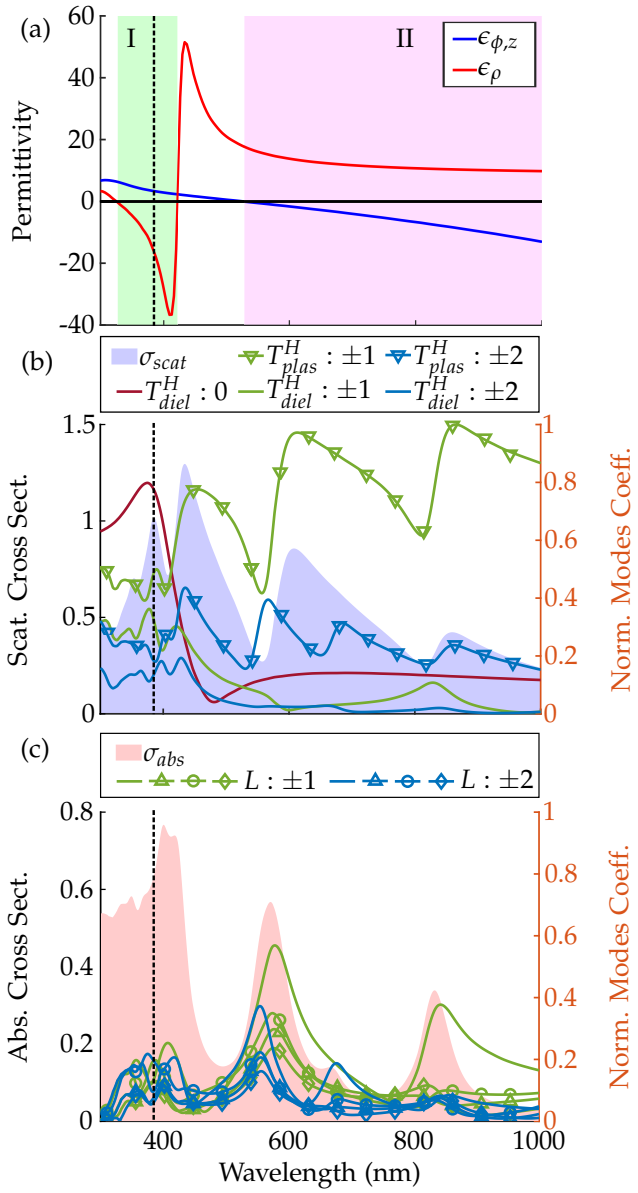

FIGURE 3: *Cylinder with diameter* 180 *nm and material with composition of silver* $p = 0.4$. *(a) Real part of the in-plane (red) and out-of-plane (blue) components of the permittivity tensor. The green and purple domain shows the domain in which the material is hyperbolic type I and II respectively. (b) Scattering cross-section (blue area) respectively to the left axis. The evolution of the coefficient* γ_m *are represented by the curve respectively to the right axis. Only the transverse modes have been represented. (c) Absorption cross-section (red area) and coefficient of the longitudinal modes. The coefficient* $|\gamma_n|$ *have been normalized by the maximum of the most important mode.*

{fig:modcoef}

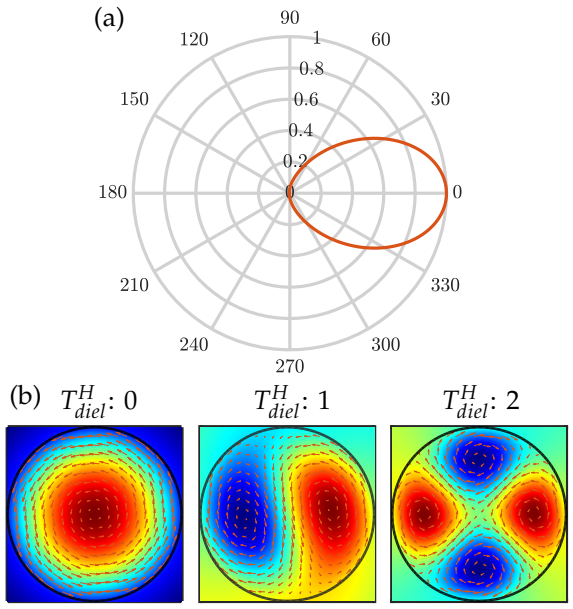

FIGURE 4: *(a) Scattering diagram of cylinder with diameter* 180 *nm at wavelength* 389 *nm for a composition of silver in the material of* $p = 0.4$ *corresponding to the vertical dashed line in Fig. 3. (b) Magnetic field (surface) and displacement current density (arrows) for the modes* $T^H_{diel} : 0$, $T^H_{diel} : 1$ *and* $T^H_{diel} : 2$.

{fig:scatpat}

A Generalized Normal Modes Expansion for anisotropic scatterers

{sec:genome}

A.1 Lippman-Schwinger equation and symmetrization

{sec:lippman}

Let us consider an infinite inclusion with an anisotropic homogeneous permittivity tensor $\bar{\bar{\epsilon}}$ embedded in an isotropic homogeneous medium ϵ_b, Fig. 5. We define $\Delta\bar{\bar{\epsilon}} \equiv \bar{\bar{\epsilon}} - \epsilon_b$, the permittivity difference between the inclusion and the background.

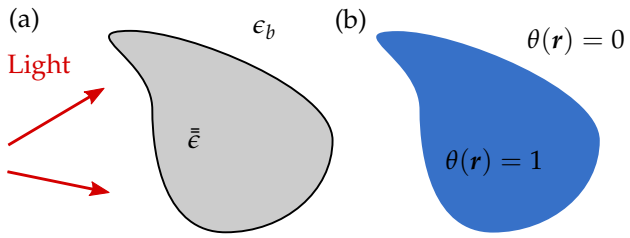

FIGURE 5: *The inclusion is an arbitrary shaped structure made of an anisotropic material. (a) The permittivity of the inclusion, $\bar{\bar{\epsilon}}$ is a tensor. The background is an isotropic medium with permittivity ϵ_b.(b) Function $\theta(\boldsymbol{r})$ defined by* 1 *inside the inclusion, blue domain, and* 0 *outside, white domain.*

{fig:schm}

For monochromatic wave illumination, Maxwell's equations inside the inclusion lead to the wave equation:

$$\nabla \times \nabla \times \boldsymbol{E}(\boldsymbol{r}) - k^2\, \bar{\bar{\epsilon}}\, \boldsymbol{E}(\boldsymbol{r}) \quad = \quad j\omega\mu_0 \boldsymbol{J}(\boldsymbol{r}), \tag{10}$$

{eq:waveqcyl}

and outside,

$$\nabla \times \nabla \times \boldsymbol{E}(\boldsymbol{r}) - k^2\, \epsilon_b\, \boldsymbol{E}(\boldsymbol{r}) \quad = \quad j\omega\mu_0 \boldsymbol{J}(\boldsymbol{r}), \tag{11}$$

{eq:waveqcylout}

with k the wavevector in free space, ω the frequency, μ_0 the free space permeability and $\boldsymbol{J}$ the free current. Subtracting the term $k^2\epsilon_b\boldsymbol{E}$ from both sides of Eq. (10), we introduce the function $\theta(\boldsymbol{r})$ that is 1 inside the inclusion and 0 outside (see Fig. 5) and we merge Eqs. (10)-(11) into

$$\nabla \times \nabla \times \boldsymbol{E}(\boldsymbol{r}) - k^2\epsilon_b \boldsymbol{E}(\boldsymbol{r}) \quad = \quad j\omega\mu_0 \boldsymbol{J}(\boldsymbol{r}) + k^2\theta(\boldsymbol{r})\, \Delta\bar{\bar{\epsilon}}\, \boldsymbol{E}(\boldsymbol{r}). \tag{12}$$

{eq:waveqgen}

that is true in all region of space. With the expression Eq. (12), we treat the inclusion as a source (or depolarization current) induced by the permittivity contrast. The free space Green's tensor $\bar{\bar{G}}_0(\boldsymbol{r}, \boldsymbol{r}')$ associated with the left hand side of Eq. (12) is the solution of [51]

$$\nabla \times \nabla \times \bar{\bar{G}}_0(\boldsymbol{r}, \boldsymbol{r}') - k^2\epsilon_b \bar{\bar{G}}_0(\boldsymbol{r}, \boldsymbol{r}') \quad = \quad \bar{\bar{I}}\delta(\boldsymbol{r} - \boldsymbol{r}'), \tag{13}$$

{eq:waveqgreen}

where $\bar{\bar{I}}$ is the identity matrix. The free space Green's tensor can be used to write down a formal solution of equation (12) as

$$\boldsymbol{E}(\boldsymbol{r}) \quad = \quad \boldsymbol{E}_0(\boldsymbol{r}) + \hat{\Gamma}\hat{C}\boldsymbol{E}(\boldsymbol{r}), \qquad \hat{\Gamma}\hat{C}\boldsymbol{E}(\boldsymbol{r}) \equiv k^2 \int_V \theta(\boldsymbol{r}')\, \bar{\bar{G}}_0(\boldsymbol{r}, \boldsymbol{r}')\, \Delta\bar{\bar{\epsilon}}\, \boldsymbol{E}(\boldsymbol{r}')d\boldsymbol{r}', \tag{14}$$

{eq:solwaveq}

usually referred to as the Lippman-Schwinger equation. It was obtained by convolving the free-space Green's tensor with the two terms on the right-hand-side of Eq. (12). The first one

{eq:e0}
$$\boldsymbol{E}_0(\boldsymbol{r}) \quad = \quad \int_V \bar{\bar{G}}_0(\boldsymbol{r},\boldsymbol{r}')\boldsymbol{J}(\boldsymbol{r}')d\boldsymbol{r}', \tag{15}$$

In the case of an isotropic inclusion, the permittivity tensor is diagonal with identical diagonal terms, $\Delta\bar{\bar{\epsilon}} = \Delta\epsilon\bar{\bar{I}}$. Then, the permittivity in Eq. (14) can be factorized out of the integral and the new operator becomes

{eq:solwaveq2}
$$\hat{\Gamma}\boldsymbol{E}(\boldsymbol{r}) = k^2\Delta\epsilon \int_V \theta(\boldsymbol{r}')\, \bar{\bar{G}}_0(\boldsymbol{r},\boldsymbol{r}')\boldsymbol{E}(\boldsymbol{r}')d\boldsymbol{r}'. \tag{16}$$

Here, we can make two observations. First, the linear operator $\hat{\Gamma}$ is symmetric [19] and, thus, defines a set of orthogonal eigenmodes for the inner product defined by

{eq:inprod}
$$\int \theta(\boldsymbol{r})\boldsymbol{E}_n^{\dagger}(\boldsymbol{r})\boldsymbol{E}_m(\boldsymbol{r})d\boldsymbol{r} = \delta_{nm}, \tag{17}$$

where the superscript † is for the adjoint mode and implies the transposition. Secondly, Eq. (16) is written in its integral form but the differential form is also known, it is the source-free Helmholtz equation,

{eq:helmeq}
$$\nabla\times\nabla\times\boldsymbol{E}(\boldsymbol{r}) - k^2\,\epsilon_b\,\boldsymbol{E}(\boldsymbol{r}) \quad = \quad k^2\theta(\boldsymbol{r})\Delta\epsilon\boldsymbol{E}(\boldsymbol{r}). \tag{18}$$

For simple geometries (e.g., a slab, cylinder, sphere), a set of orthogonal modes and their associated adjoints can be constructed by using the pre-knowledge of the functional form of the eigenmodes [22, 23, 24, 25, 19] and employing an efficient complex root search [26]. In more complicated geometries, one can always resort to a numerical approach [19, 27]. Clusters of scatterers can be treated with minimal overhead computations by the rigorous hybridization approach described in [28, 29, 20].

The complication associated with anisotropic materials now becomes clear - the permittivity and the Green's tensors do not commute in general. Thus, the linear operator defined in Eq. (14) is non-symmetric. Therefore, the modes $\tilde{E}_\mu$ of the operator $\hat{\Gamma}\hat{C}$ associated to the eigenvalue $\tilde{s}_\mu$ and defined by

{eq:eigtargmode}
$$\tilde{s}_\mu\tilde{\boldsymbol{E}}_\mu = k^2\int \theta(\boldsymbol{r}')\bar{\bar{G}}_0(\boldsymbol{r},\boldsymbol{r}')\Delta\bar{\bar{\epsilon}}\boldsymbol{E}_\mu(\boldsymbol{r}')d\boldsymbol{r}', \tag{19}$$

do not, necessarily, define a orthogonal base for the inner product Eq. (17).

To overcome this issue, we use the symmetry property of the permittivity tensor [52] to symmetrize the operator $\hat{\Gamma}\hat{C}$ and define a new inner product that satisfy the orthogonality relation of the modes $\tilde{\boldsymbol{E}}_\mu$. Specifically, we introduce the square roots $\bar{\bar{R}}$ of the permittivity tensor [53], $\Delta\bar{\bar{\epsilon}} = \bar{\bar{R}}\bar{\bar{R}}$ and we multiply it of the left of Eq. (19), which gives

{eq:eigvaleqE}
$$\tilde{s}_\mu\bar{\bar{R}}\tilde{\boldsymbol{E}}_\mu(\boldsymbol{r}) \quad = \quad k^2\int_V \theta(\boldsymbol{r}')\bar{\bar{R}}\,\bar{\bar{G}}_0(\boldsymbol{r},\boldsymbol{r}')\,\bar{\bar{R}}\,\bar{\bar{R}}\tilde{\boldsymbol{E}}_\mu(\boldsymbol{r}')d\boldsymbol{r}'. \tag{20}$$

Introducing a temporary notation, $\boldsymbol{F} \equiv \bar{\bar{R}}\boldsymbol{E}$, Eq. (20) becomes

{eq:eigvaleqF}
$$\tilde{s}_\mu\tilde{\boldsymbol{F}}_\mu(\boldsymbol{r}) \quad = \quad k^2\int_V \theta(\boldsymbol{r}')\bar{\bar{R}}\,\bar{\bar{G}}_0(\boldsymbol{r},\boldsymbol{r}')\,\bar{\bar{R}}\,\tilde{\boldsymbol{F}}_\mu(\boldsymbol{r}')d\boldsymbol{r}'. \tag{21}$$

The new operator defined of the right hand side of Eq. (21) is symmetric so its right eigenmodes, $\tilde{\boldsymbol{F}}_\mu$, define a complex orthogonal base for the inner product,

{eq:newinprodF}
$$\int \theta(\boldsymbol{r}) \boldsymbol{F}_\nu^\dagger(\boldsymbol{r}) \boldsymbol{F}_\mu(\boldsymbol{r}) d\boldsymbol{r} = \delta_{nm}. \tag{22}$$

Therefore, from this analysis we deduce that the inner product satisfied by the modes $\tilde{\boldsymbol{E}}_\mu$ of the operator $\hat{\Gamma}\hat{C}$ is

{eq:newinprod}
$$\int \theta(\boldsymbol{r}) \boldsymbol{E}_\nu^\dagger(\boldsymbol{r}) \Delta\bar{\bar{\epsilon}} \boldsymbol{E}_\mu(\boldsymbol{r}) d\boldsymbol{r} = \delta_{nm}. \tag{23}$$

Using the bra-ket notation, the inner product is noted $\langle \boldsymbol{E}_\nu | \hat{C} | \boldsymbol{E}_\mu \rangle$ where $\hat{C}$ is the operator associated with the step function θ and the permittivity tensor $\Delta\bar{\bar{\epsilon}}$ and Eq. (19) can be written as

{eq:eigvaleqFbr}
$$\tilde{s}_\mu \, |E_\mu\rangle \quad = \quad \hat{\Gamma}\hat{C} \, |E_\mu\rangle \, . \tag{24}$$

At this point, the differential form of equation (24) remains unknown, and it is complicated to directly construct the set of orthogonal modes for anisotropic materials. As a consequence, we choose to utilize the known modes of an isotropic inclusion with the same shape to construct an orthonormal set of new modes using the re-expansion method [21].

A.2 The re-expansion method

{sec:reexp}

A.2.1 Derivation of the re-expansion eigenvalue problem

Let us consider an inclusion composed of material with an isotropic permittivity ϵ_m and having the exact same shape as our anisotropic inclusion of interest. In absence of free current sources, the vector Helmholtz equation for the isotropic case, Eq. (12), becomes

{eq:waveqiso}
$$\nabla \times \nabla \times \boldsymbol{E}_m(\boldsymbol{r}) - k^2 \epsilon_b \boldsymbol{E}_m(\boldsymbol{r}) \quad = \quad \frac{1}{s_m} \theta(\boldsymbol{r}) k^2 \epsilon_b \boldsymbol{E}_m(\boldsymbol{r}), \tag{25}$$

where $s_m = \frac{\epsilon_b}{\epsilon_m - \epsilon_b}$, the Bergman spectral parameter [54] corresponds to the eigenvalue associated with the mode $\boldsymbol{E}_m$ solution of

{eq:solem}
$$s_m \boldsymbol{E}_m(\boldsymbol{r}) \quad = \quad k^2 \epsilon_b \int_V \theta(\boldsymbol{r}') \bar{\bar{G}}_0(\boldsymbol{r}, \boldsymbol{r}') \boldsymbol{E}_m(\boldsymbol{r}') d\boldsymbol{r}'. \tag{26}$$

Since $\boldsymbol{E}_m$ is a complete set inside the inclusion [19], we decompose the modes of the anisotropic inclusion, also called target modes, in terms of modes of the isotropic inclusion

{eq:rexpanmodE}
$$\tilde{\boldsymbol{E}}_\mu(\boldsymbol{r}) \quad = \quad \sum_m c_{\mu,m} \boldsymbol{E}_m(\boldsymbol{r}). \tag{27}$$

These modes satisfy

{eq:waveqtargmode}
$$\nabla \times \nabla \times \tilde{\boldsymbol{E}}_\mu(\boldsymbol{r}) - k^2 \epsilon_b \tilde{\boldsymbol{E}}_\mu(\boldsymbol{r}) = \frac{1}{\tilde{s}_\mu} \theta(\boldsymbol{r}) k^2 \Delta\bar{\bar{\epsilon}} \tilde{\boldsymbol{E}}_\mu(\boldsymbol{r}). \tag{28}$$

Inserting the decomposition of the target modes (27) in Eq. (28) yields

{eq:rexpan1}
$$\sum_m c_{\mu,m} \left[\nabla \times \nabla \times \boldsymbol{E}_m(\boldsymbol{r}) - k^2 \epsilon_b \boldsymbol{E}_m(\boldsymbol{r}) \right] \quad = \quad \frac{1}{\tilde{s}_\mu} \theta(\boldsymbol{r}) k^2 \Delta\bar{\bar{\epsilon}} \sum_m c_{\mu,m} \boldsymbol{E}_m(\boldsymbol{r}). \tag{29}$$

We replace the terms in the brackets in the left-hand-side of Eq. (29) by the right-hand-side of Eq. (25) leading to

{eq:rexpan2}
$$\sum_m c_{\mu,m}\frac{1}{s_m}\theta(\boldsymbol{r})k^2\epsilon_b\boldsymbol{E}_m(\boldsymbol{r}) \quad = \quad \frac{1}{\tilde{s}_\mu}\theta(\boldsymbol{r})k^2\Delta\bar{\bar{\epsilon}}\sum_m c_{\mu,m}\boldsymbol{E}_m(\boldsymbol{r}). \tag{30}$$

Then, we project Eq. (30) along one of the basis mode $\boldsymbol{E}_n$ using the orthogonality relationship Eq. (17), yielding to

{eq:rexpan3}
$$c_{\mu,n}\frac{1}{s_n}\epsilon_b = \frac{1}{\tilde{s}_\mu}\sum_m c_{\mu,n}\int\theta(\boldsymbol{r})\boldsymbol{E}_n^\dagger(\boldsymbol{r})\Delta\bar{\bar{\epsilon}}\boldsymbol{E}_m(\boldsymbol{r})d\boldsymbol{r}. \tag{31}$$

We recognize on the right-hand-side of Eq. (31) the overlap integral between the modes $\boldsymbol{E}_n$ and $\boldsymbol{E}_m$,

{eq:vmn}
$$v_{mn} \quad = \quad \int_V \theta(\boldsymbol{r})\boldsymbol{E}_n^\dagger(\boldsymbol{r})\cdot\Delta\bar{\bar{\epsilon}}\,\boldsymbol{E}_m(\boldsymbol{r})d\boldsymbol{r}, \tag{32}$$

that represents the mixing between the modes of the isotropic inclusion due to the anisotropy of the material. We rewrite Eq. (31) as

{eq:rexpan4}
$$\tilde{s}_\mu c_{\mu,n} \quad = \quad \frac{s_n}{\epsilon_b}\sum_m c_{\mu,m}v_{mn}, \tag{33}$$

which using matrix notation is

{eq:rexpaneig}
$$\tilde{s}_\mu\boldsymbol{c}_\mu \quad = \quad \bar{\bar{S}}\,\bar{V}\boldsymbol{c}_\mu, \tag{34}$$

with $\bar{\bar{S}} = \frac{1}{\epsilon_b}\,\mathrm{diag}[s_m]$ and $\bar{V} = [v_{mn}]$, the overlap integral matrix.

Eq. (34) is key to understand how the modes of an anisotropic inclusion differ from the modes of an isotropic inclusion. One can easily verify that in the case of an isotropic inclusion, the overlap matrix is diagonal due to the absence of coupling between the modes. Eq. (34) then reduces to $\tilde{s}_\mu\boldsymbol{c}_\mu = \frac{\Delta\epsilon}{\epsilon_b}\,\mathrm{diag}[s_m]\boldsymbol{c}_\mu$ which is trivially solved by $\tilde{s}_\mu = \frac{\epsilon_i-\epsilon_b}{\epsilon_b}s_\mu$ and unitary vectors $\boldsymbol{c}_\mu$ (i.e. the new base of modes is identical to the previous one, $\tilde{\boldsymbol{E}}_\mu = \boldsymbol{E}_\mu$). On the other hand, for an anisotropic inclusion, the overlap matrix may not be diagonal due to the mixing between the modes induced by the anisotropy. For example, the presence of off-diagonal terms in the permittivity tensor may induced mixing between modes that would be symmetry forbidden in the isotropic case.

A.2.2 The total electric field

Using the bra-ket notation introduced in Section A.1, Eq. (14) can be rewritten as

{eq:sole}
$$|E\rangle \quad = \quad |E_0\rangle + \hat{\Gamma}\hat{C}\,|E\rangle\,. \tag{35}$$

By inverting this relation, we can express the field $|E\rangle$ as a function of the incident field, namely,

{eq:soleinv}
$$|E\rangle \quad = \quad \left(1-\hat{\Gamma}\hat{C}\right)^{-1}|E_0\rangle\,. \tag{36}$$

The set of eigenmodes $\tilde{\boldsymbol{E}}_\mu$ forms a complete orthonormal base inside the inclusion [19] for the inner product (23), therefore, we can write the following identity

{eq:id}
$$\bar{\bar{I}} \quad = \quad \sum_\mu |\tilde{E}_\mu\rangle\,\langle\tilde{E}_\mu|\,\hat{C}. \tag{37}$$

By multiplying on the right by $|E\rangle$ we have inside the inclusion

{eq:idE}
$$|E\rangle \quad = \quad \sum_{\mu} |\tilde{E}_\mu\rangle \, \langle \tilde{E}_\mu | \hat{C} | E \rangle \, . \tag{38}$$

We substitute the term $|E\rangle$ on the right-hand-side of Eq. (38) by its expression (36).

{eq:idE2}
$$|E\rangle \quad = \quad \sum_{\mu} |\tilde{E}_\mu\rangle \, \langle \tilde{E}_\mu | \hat{C} (1 - \hat{\Gamma}\hat{C})^{-1} | E_0 \rangle \, . \tag{39}$$

The operator in the brackets can be rearranged in

{eq:opcom}
$$\hat{C}(1 - \hat{\Gamma}\hat{C})^{-1} = (1 - \hat{\Gamma}\hat{C})^{-1}\hat{C}. \tag{40}$$

We, then, apply the operator $(1 - \hat{\Gamma}\hat{C})^{-1}$ to the adjoint $\langle \tilde{E}_\mu|$ so that we have

{eq:soleInclu}
$$|E\rangle \quad = \quad \sum_{\mu} |\tilde{E}_\mu\rangle \, \frac{1}{1 - \tilde{s}_\mu} \, \langle \tilde{E}_\mu | \hat{C} | E_0 \rangle \, , \tag{41}$$

and in the total space by inserting (41) into (35)

{eq:solEtotal}
$$|E\rangle \quad = \quad |E_0\rangle + \sum_{\mu} |\tilde{E}_\mu\rangle \, \frac{\tilde{s}_\mu}{1 - \tilde{s}_\mu} \, \langle \tilde{E}_\mu | \hat{C} | E_0 \rangle \, . \tag{42}$$

Eq. (42) gives the modal decomposition of the scattered (and total) field in terms of target modes $|\tilde{E}_\mu\rangle$. The coefficients of this decomposition are expressed by the projection $\langle \tilde{E}_\mu | \hat{C} | E_0 \rangle$ that represents the excitation of the modes by the incident source and by the detuning factor, $\frac{\tilde{s}_\mu}{1-\tilde{s}_\mu}$ [19]. The formulation (42) is similar to the one presented in [19]. However, since the target modes are a linear combination of modes of the isotropic inclusion, they may not, in general, be exactly identified by a set of integers (radial, azimuthal or longitudinal orders) such as the modes of the isotropic inclusion. One target mode can be expressed by modes with different radial azimuthal or radial orders; this may hinder the physical interpretation. For practical application and physical interpretation, it is better to re-write Eq. (42) in terms of modes $\boldsymbol{E}_m$. It supposes that we can intervert the two infinite sums, but for numerical simulations, the sums are truncated and therefore finite. Thus, we substitute Eq. (27) in Eq. (42) and regroup the terms for each modes $\boldsymbol{E}_m$. We get

{eq:soleApp}
$$|E\rangle \quad = \quad |E_0\rangle + \sum_{m}^{N} \left[\sum_{\mu}^{N} c_{\mu,m} \frac{\tilde{s}_\mu}{1 - \tilde{s}_\mu} \, \langle \tilde{E}_\mu | \hat{C} | E_0 \rangle \right] |E_m\rangle \, . \tag{43}$$

We can rewrite in

{eq:solEtot}
$$|E\rangle \quad = \quad |E_0\rangle + \sum_{m}^{N} \gamma_m \, |E_m\rangle \, . \tag{44}$$

where $\gamma_m = \sum_{\mu}^{N} c_{\mu,m} \frac{\tilde{s}_\mu}{1-\tilde{s}_\mu} \, \langle \tilde{E}_\mu | \hat{C} | E_0 \rangle$ corresponds to the total contribution of the m-th mode of the isotropic inclusion to the total field. Therefore, specific behavior such as dipolar radiation or other are clearly identified in Eq. (44). Secondly, when it comes to compare the results from different set of simulations, using the base of isotropic modes ensures that the results are comparable.

A.2.3 Orthogonality and Adjoint Modes

To complete GENOME, the adjoints of the target modes have to be determined. As presented in Appendix B, the adjoint of the modes of the isotropic inclusion have been fully determined and they can be found by applying the following transformation

{eq:adjiso}
$$\boldsymbol{E}_m^\dagger(r,\phi,z) = \boldsymbol{E}_m(r,-\phi,-z). \tag{45}$$

Therefore, to fully determine the adjoint of the target modes, we only have to express the coefficients $b_{\mu,m}$ of the linear decomposition of the adjoint mode in the base of modes of the isotropic inclusion

{eq:rexpanadj}
$$\boldsymbol{E}_\mu^\dagger(\boldsymbol{r}) \quad = \quad \sum_m b_{\mu,m}\boldsymbol{E}_m^\dagger(\boldsymbol{r}). \tag{46}$$

The coefficient $b_{\mu,m}$ are unknown and to find how they are related to the coefficient $c_{\mu,m}$, one can derive, similarly to Section A.2, an equivalent relation to Eq. (34) for the adjoint mode

{eq:rexpaneiga}
$$\tilde{s}_\mu \boldsymbol{b}_\mu \quad = \quad \boldsymbol{b}_\mu \bar{\bar{V}}\bar{\bar{S}}. \tag{47}$$

The overlap integral matrix and the matrix of eigenvalue of isotropic inclusion do not commute, in general, which means that the linear coefficients of the adjoint mode decomposition are not the left eigenvectors of Eq. (34). However, to avoid the resolution of (34) and (47), we can resolve the eigenvalue problem of the symmetrized matrix $\bar{\bar{S}}^{\frac{1}{2}}\bar{\bar{V}}\bar{\bar{S}}^{\frac{1}{2}}$, with $\bar{\bar{S}}^{\frac{1}{2}} = \frac{1}{\sqrt{\epsilon_b}}\,\mathrm{diag}[\sqrt{s_m}]$ [21]. We emphasize depending on the base of function that is used to describe the rotational symmetries, the overlap integral matrix, $\bar{\bar{V}}$, may not be necessarily symmetric. To ensure, the symmetry property of the overlap integral matrix, it is beneficial to describe the rotational symmetries with the base of trigonometric functions $(\cos m\phi, \sin m\phi)$ instead of the exponential functions $(e^{im\phi}, e^{-im\phi})$.

B Adjoint modes and orthogonality for isotropic materials

{sec:adjoint}

The adjoint field $\boldsymbol{E}_n^\dagger(\boldsymbol{r})$ in (32) is not necessarily the complex conjugate field $\boldsymbol{E}_n^*(\boldsymbol{r})$, which is the familiar form of $\langle E_n|$ for a self-adjoint or Hermitian operator. Instead, the adjoint field is identical to the direct field itself, a property which stems from the Green's function operator $\hat{\Gamma}$, which is symmetric but not necessarily real.

To show this property of the adjoint field, we recall its purpose: it is defined such that the direct and adjoint modes form a biorthogonal set,

$$\langle E_m|\,\hat{\theta}\,|E_n\rangle = \int \boldsymbol{E}_m^\dagger(\boldsymbol{r})\cdot\theta(\boldsymbol{r})\boldsymbol{E}_n(\boldsymbol{r})\,d\boldsymbol{r} = \delta_{mn}, \tag{48}$$

with $\theta(\boldsymbol{r})$ serving as the weight function. The proof of this property in fact demonstrates that the adjoint field is identical to the direct field. To proceed, we evaluate the following expression two

different ways, beginning with

$$\begin{aligned}\langle E_n|\,\hat{\theta}\hat{\Gamma}\hat{\theta}\,|E_m\rangle &= \iint \boldsymbol{E}_n^\dagger(\boldsymbol{r})\cdot\theta(\boldsymbol{r})\bar{\bar{G}}_0(|\boldsymbol{r}-\boldsymbol{r}'|)\theta(\boldsymbol{r}')\boldsymbol{E}_m(\boldsymbol{r}')\,d\boldsymbol{r}d\boldsymbol{r}' \\ &= \int \boldsymbol{E}_n^\dagger(\boldsymbol{r})\cdot\theta(\boldsymbol{r})\int \bar{\bar{G}}_0(|\boldsymbol{r}-\boldsymbol{r}'|)\theta(\boldsymbol{r}')\boldsymbol{E}_m(\boldsymbol{r}')\,d\boldsymbol{r}d\boldsymbol{r}' \\ &= s_m\int \boldsymbol{E}_n^\dagger(\boldsymbol{r})\cdot\theta(\boldsymbol{r})\boldsymbol{E}_m(\boldsymbol{r})\,d\boldsymbol{r} \\ &= s_m\,\langle E_n|\,\hat{\theta}\,|E_m\rangle\,.\end{aligned} \tag{49}$$

So far, we have not specified what $\boldsymbol{E}_n^\dagger(\boldsymbol{r})$ is, except that it exists. Now consider the alternative way of evaluating,

$$\begin{aligned}\langle E_n|\,\hat{\theta}\hat{\Gamma}\hat{\theta}\,|E_m\rangle &= \iint \boldsymbol{E}_n^\dagger(\boldsymbol{r})\cdot\theta(\boldsymbol{r})\bar{\bar{G}}_0(|\boldsymbol{r}-\boldsymbol{r}'|)\,d\boldsymbol{r}\theta(\boldsymbol{r}')\boldsymbol{E}_m(\boldsymbol{r}')\,d\boldsymbol{r}' \\ &= \int\left[\int \bar{\bar{G}}_0^{\intercal}(|\boldsymbol{r}-\boldsymbol{r}'|)\theta(\boldsymbol{r})\boldsymbol{E}_n^\dagger(\boldsymbol{r})\,d\boldsymbol{r}\right]\cdot\theta(\boldsymbol{r}')\boldsymbol{E}_m(\boldsymbol{r}')\,d\boldsymbol{r}' \\ &= s_n\int \boldsymbol{E}_n^\dagger(\boldsymbol{r}')\cdot\theta(\boldsymbol{r}')\boldsymbol{E}_m(\boldsymbol{r}')\,d\boldsymbol{r}' \\ &= s_n\,\langle E_n|\,\hat{\theta}\,|E_m\rangle\,.\end{aligned} \tag{50}$$

which follows because the dot product implies transposition, $\boldsymbol{a}\cdot\boldsymbol{b}\equiv\boldsymbol{a}^{\intercal}\boldsymbol{b}$. We may simplify the square brackets with one assumption,

{eq:adjoint}
$$\boldsymbol{E}_m^\dagger(\boldsymbol{r}) = \boldsymbol{E}_m(\boldsymbol{r}), \tag{51}$$

that adjoint is simply the original field. Then, the square brackets satisfies the defining eigenvalue equation due to the symmetry of the Green's tensor both under transposition and the interchange of $\boldsymbol{r}$ and $\boldsymbol{r}'$,

$$\bar{\bar{G}}_0^{\intercal}(|\boldsymbol{r}-\boldsymbol{r}'|) = \bar{\bar{G}}_0(|\boldsymbol{r}'-\boldsymbol{r}|). \tag{52}$$

Combining these results, we obtain

$$\langle E_n|\,\hat{\theta}\hat{\Gamma}\hat{\theta}\,|E_m\rangle = s_n\,\langle E_n|\,\hat{\theta}\,|E_m\rangle = s_m\,\langle E_n|\,\hat{\theta}\,|E_m\rangle\,, \tag{53}$$

{eq:orthoproof}
$$(s_n - s_m)\,\langle E_n|\,\hat{\theta}\,|E_m\rangle = 0, \tag{54}$$

so eigenvectors belonging to different eigenvalues are orthogonal. We have also identified the form of the adjoint necessary to yield orthogonality. These properties are guarenteed by the complex symmetric nature of the Green's tensor. However, (54) is silent on the orthogonality of degenerate modes that have the same eigenvalue. Indeed, such modes will not automatically be orthogonal, and it often needs to be enforced by some other means. One case in particular is relevant to this manuscript: degeneracy due to symmetry.

For modes that are degenerate due to symmetry, one way to obtain an orthogonal set is by blind application of say the Gram-Schmidt algorithm, using the integral in (54) as the metric. The resulting eigenmodes will be orthogonal, but typically will not have any recognisable symmetry properties upon visual inspection. This is not problematic for numerical purposes, but can hinder physical interpretation. Alternatively, we can consider the set of symmetry operations that leave

the structure invariant. The eigenmodes $\boldsymbol{E}_m$ of Green's tensor in (26) will simultaneously be eigenmodes of these symmetry operations. Just as the properties of the operator (26) impose an orthogonality relation on its eigenmodes, so too do the symmetry operations on its eigenmodes. While the operator (26) is unable to establish orthogonality among a symmetry degenerate set, the symmetry operations can. In practice, the formal properties of the symmetry operations do not need to be analyzed. Instead, orthogonality can be established, after a degenerate set of eigenmodes has been found, by choosing the appropriate linear combination such that they are also eigenmodes of the symmetry operations. This process is possible for many finite symmetries by relying only on intuition. For more complex symmetries, the tools of group theory can be used as an aid.

Several types of symmetry deserve special mention. These are continuous rotational symmetry, continuous translational symmetry, and discrete translational symmetry, also known as periodicity. The eigenmodes of these symmetry operations are known to have the spatial variation $e^{im\phi}$, e^{ikz}, and $e^{i\boldsymbol{k}_B R}$, with the latter applicable to any lattice point R. However, a problem arises when these spatial variations are inserted into the integral of (54), and integration is performed along the direction of symmetry. The result is zero, for example, $\int e^{im\phi}e^{im\phi}\,d\phi = 0$, arriving at the paradoxical conclusion that each mode is orthogonal to itself. This can be remedied by using the $\{\cos m\phi, \sin m\phi\}$ basis instead. Since we wish to use the $e^{im\phi}$ eigenmodes, we need to embark on a brief detour into their properties. All symmetry operators are orthogonal operators, satisfying the property $\langle \hat{S}\psi\rangle\, \hat{S}\phi = \langle\psi\rangle\, \phi$. This leads to the more familiar case of the adjoint mode being the complex conjugate, $\psi^\dagger = \psi^*$, or alternatively $\psi^\dagger(\boldsymbol{r}) = \psi(-\boldsymbol{r})$. This conflicts with the definition (51), so a hybrid definition of the adjoint becomes necessary for these three symmetries. For example, if the geometry possesses both continuous rotational symmetry in θ and continuous translational symmetry in z, we may define the adjoint as

$$\boldsymbol{E}_m^\dagger(r,\phi,z) = \boldsymbol{E}_m(r,-\phi,-z). \tag{55}$$

C Conditions on the materials

{sec:mat}

In Section A.1, we introduced the square roots of the permittivity tensor $\bar{\bar{R}}$ in order to define the inner product Eq. (23). This tensor is defined and symmetric if the permittivity tensor is diagonalizable by a series of rotations, i.e.,

{eq:diagesp}

$$\Delta\bar{\bar{\epsilon}} = \bar{\bar{P}}^{-1}\bar{\bar{D}}\bar{\bar{P}}, \qquad \bar{\bar{P}}^{-1} = \bar{\bar{P}}^{\intercal} \tag{56}$$

Eq. (56) is valid for biaxial anisotropic materials where the principle axes of the material form an orthogonal base. In these cases, we define the roots by $\bar{\bar{R}} = \bar{\bar{P}}^{\intercal}\bar{\bar{D}}^{\frac{1}{2}}\bar{\bar{P}}$; clearly, $\bar{\bar{R}}$ is symmetric. Conversely, for triclinic [55], monoclinic [56], trigonal and hexagonal crystals, the permittivity tensor is diagonal in a non-orthogonal base of vectors, i.e., Eq. (56) holds with $\bar{\bar{P}}^{-1} \neq \bar{\bar{P}}^{\intercal}$, so the roots of the permittivity tensor are defined but may not be symmetric. Furthermore, for non-reciprocal materials, the permittivity tensor is not symmetric [57]. For example, with magneto-optic materials, also called gyrotropic materials, when there is no loss the permittivity tensor is complex and Hermitian [58]. More precisely, the off-diagonal terms of the permittivity tensor are pure imaginary with opposite sign one to another, $\epsilon_{xy} = -\epsilon_{yx} = i\epsilon_g$ [59]. Thus, the permittivity tensor satisfies Eq. (56) with instead $\bar{\bar{P}}^{-1} = \bar{\bar{P}}^{*,\intercal}$. Therefore, the square roots of the permittivity tensor are Hermitian, so not symmetric. We emphasize that besides the condition (56), there is no

restriction on the imaginary part of the permittivity tensor so that scattering properties of lossy materials can be studied. From now on, we treat only materials satisfying Eq. (56).

D Overlap integrals

{sec:ovint}

The overlap integral between the modes is calculated via

{eq:ovint}
$$v_{mn} = \int \theta(\boldsymbol{r}) \boldsymbol{E}_n^\dagger(\boldsymbol{r}) \cdot \Delta\bar{\bar{\epsilon}} \boldsymbol{E}_m(\boldsymbol{r}) d\boldsymbol{r} \tag{57}$$

So, the integrand in the right-hand-side of (57) is a dot product of two vectors $\boldsymbol{E}_n^\dagger$ and $\Delta\bar{\bar{\epsilon}}\boldsymbol{E}_m$ that are expressed in the cylindrical base. However, for the following derivation, it is easier to expressed them in the rotational basis

{eq:rotbas}
$$\hat{\boldsymbol{e}}_+ = \frac{1}{\sqrt{2}}(e^{i\phi}\hat{\boldsymbol{e}}_\rho + ie^{i\phi}\hat{\boldsymbol{e}}_\phi) \qquad \hat{\boldsymbol{e}}_- = \frac{1}{\sqrt{2}}(e^{-i\phi}\hat{\boldsymbol{e}}_\rho - ie^{-i\phi}\hat{\boldsymbol{e}}_\phi) \tag{58}$$

D.1 Transverse modes

From [44], we express the m-modes of the electric field inside the cylinder in a cylindrical base

{eq:Er}
$$E_r = \left[C_m^E \frac{i\beta}{\alpha_m} J_m'(\alpha_m r) - C_m^H \frac{mk\mu}{r\alpha_m^2} J_m(\alpha_m r)\right] e^{im\phi} e^{i\beta z} \tag{59}$$

{eq:Eth}
$$E_\phi = \left[-C_m^E \frac{m\beta}{r\alpha_m^2} J_m(\alpha_m r) - C_m^H \frac{ik\mu}{\alpha_m} J_m'(\alpha_m r)\right] e^{im\phi} e^{i\beta z} \tag{60}$$

{eq:Ez}
$$E_z = C_m^E J_m(\alpha_m r) e^{im\phi} e^{i\beta z} \tag{61}$$

To express this mode in the rotational basis, we project $\Delta\bar{\bar{\epsilon}}\boldsymbol{E}_m$ onto $\hat{\boldsymbol{e}}_+$ yielding

$$E_m^+ = \left[\frac{(\epsilon_\rho - \epsilon_{\phi,z})}{2} C_m^- J_{m-1}(\alpha_m r) + \frac{(\epsilon_\rho + \epsilon_{\phi,z})}{2} C_m^+ J_{m+1}(\alpha_m r)\right] e^{i(m+1)\phi} e^{i\beta z}$$

where we have defined the coefficient,

$$C_m^- = \frac{1}{\alpha_m\sqrt{2}}(i\beta C_m^E - k\mu C_m^H) \tag{62}$$

$$C_m^+ = -\frac{1}{\alpha_m\sqrt{2}}(i\beta C_m^E + k\mu C_m^H) \tag{63}$$

In a similar way, we project the $\Delta\bar{\bar{\epsilon}}\boldsymbol{E}_m$ onto $\hat{\boldsymbol{e}}_-$ and we obtain

$$E_m^- = \left[\frac{(\epsilon_\rho + \epsilon_{\phi,z})}{2} C_m^- J_{m-1}(\alpha_m r) + \frac{(\epsilon_\rho - \epsilon_{\phi,z})}{2} C_m^+ J_{m+1}(\alpha_m r)\right] e^{i(m-1)\phi} e^{i\beta z} \tag{64}$$

The adjoint form of the modes is written as [44]

{eq:adj}
$$E_n^\dagger = \left[C_n^E J_n(\alpha_n r) e^{-in\phi}\hat{\boldsymbol{z}} + C_n^{\dagger,+} J_{n-1}(\alpha_n r) e^{-i(n-1)\phi}\hat{\boldsymbol{e}}_+ + C_n^{\dagger,-} J_{n+1}(\alpha_n r) e^{-i(n+1)\phi}\hat{\boldsymbol{e}}_-\right] e^{-i\beta z} \tag{65}$$

where

{eq:cdag}
$$C_n^{\dagger,+} = -C_n^- \qquad C_n^{\dagger,-} = -C_n^+. \tag{66}$$

D.2 Longitudinal modes

The longitudinal modes are expressed [21] by

$$E_r = \frac{1}{2} L_{mn}\alpha_{mn}[J_{m-1}(\alpha_{mn}r) - J_{m+1}(\alpha_{mn}r)]e^{im\phi}e^{i\beta z} \quad (67)$$

$$E_\phi = imL_{mn}\frac{J_m(\alpha_{mn}r)}{r}e^{im\phi}e^{i\beta z} \quad (68)$$

$$E_z = i\beta L_{mn}J_m(\alpha_{mn}r)e^{im\phi}e^{i\beta z} \quad (69)$$

So in the rotational basis,

{eq:emnp}
$$E^+_{mn} = \left[\frac{(\epsilon_\rho - \epsilon_{\phi,z})}{2}D^-_{mn}J_{m-1}(\alpha_{mn}r) + \frac{(\epsilon_{\phi,z} + \epsilon_\rho)}{2}D^+_{mn}J_{m+1}(\alpha_{mn}r)\right]e^{i(m+1)\phi}e^{i\beta z} \quad (70)$$

where

$$D^-_{mn} = \frac{L_{mn}\alpha_{mn}}{\sqrt{2}} \quad (71)$$

$$D^+_{mn} = -\frac{L_{mn}\alpha_{mn}}{\sqrt{2}} \quad (72)$$

and

{eq:elgm}
$$E^-_{mn} = \left[\frac{(\epsilon_{\phi,z} + \epsilon_\rho)}{2}D^-_{mn}J_{m-1}(\alpha_{mn}r) + \frac{(\epsilon_\rho - \epsilon_{\phi,z})}{2}D^+_{mn}J_{m+1}(\alpha_{mn}r)\right]e^{i(m-1)\phi}e^{i\beta z}. \quad (73)$$

The adjoint mode is calculated as,

{eq:emna}
$$\boldsymbol{E}^\dagger_{mn} = D^{\dagger,+}_{mn}J_{m-1}(\alpha_{mn}r)e^{-i(m-1)\phi}e^{-i\beta z}\hat{\boldsymbol{e}}_+ + D^{\dagger,-}_{mn}J_{m+1}(\alpha_{mn}r)e^{-i(m+1)\phi}e^{-i\beta z}\hat{\boldsymbol{e}}_- - i\beta L_{mn}J_m(\alpha_{mn}r)e^{-im\phi}e^{-i\beta z} \quad (74)$$

where

{eq:dmnpa}
$$D^{\dagger,+}_{mn} = D^-_{mn} \qquad D^{dagger,-}_{mn} = D^+_{mn} \quad (75)$$

D.3 Integration

We note that in the rotationnal basis, the formulation for the transverse modes and the longitudinal is equivalent if we interchange D^-_{mn} with C^-_m, D^+_{mn} with C^+_m, $i\beta L_{mn}$ with C^E_m. So, the following derivation is still valid if the modes are longitudinal or transverse. We can then proceed to the dot product in the integrand of Eq. (57), knowing that

{eq:rotbascross}
$$\hat{\boldsymbol{e}}_+ \cdot \hat{\boldsymbol{e}}_- = 1 \qquad \hat{\boldsymbol{e}}_+ \cdot \hat{\boldsymbol{e}}_+ = \hat{\boldsymbol{e}}_- \cdot \hat{\boldsymbol{e}}_- = 0. \quad (76)$$

Thus,

{eq:integr}
$$\boldsymbol{E}^\dagger_n \cdot \Delta\bar{\bar{\epsilon}}\boldsymbol{E}_m = E^{\dagger,-}_n E^+_m + E^{\dagger,+}_n E^-_m + E^{\dagger,z}_n E^z_m \quad (77)$$

The first term on the left-hand-side of the Eq. (77) is

$$\begin{aligned} E^{\dagger,-}_n E^+_m &= C^{\dagger,-}_n J_{n+1}(\alpha_n r)\left[\frac{(\epsilon_\rho - \epsilon_{\phi,z})}{2}C^-_m J_{m-1}(\alpha_m r) + \frac{(\epsilon_\rho + \epsilon_{\phi,z})}{2}C^+_m J_{m+1}(\alpha_m r)\right]e^{i(m+1)\phi}e^{-i(n+1)\phi} \\ &= \left[\frac{(\epsilon_\rho - \epsilon_{\phi,z})}{2}C^-_m C^{\dagger,-}_n J_{n+1}(\alpha_n r)J_{m-1}(\alpha_m r) + \frac{(\epsilon_\rho + \epsilon_{\phi,z})}{2}C^+_m C^{\dagger,-}_n J_{n+1}(\alpha_n r)J_{m+1}(\alpha_m r)\right] \\ &\quad \times e^{i(m+1)\phi}e^{-i(n+1)\phi} \end{aligned}$$

The second term on the left-hand-side of the Eq. (77) is

$$\begin{aligned} E_n^{\dagger,+}E_m^- &= C_n^{\dagger,+}J_{n-1}(\alpha_n r)\left[\frac{(\epsilon_\rho-\epsilon_{\phi,z})}{2}C_m^+J_{m+1}(\alpha_m r)+\frac{(\epsilon_\rho+\epsilon_{\phi,z})}{2}C_m^-J_{m-1}(\alpha_m r)\right]e^{i(m-1)\phi}e^{-i(n-1)\phi} \\ &= \left[\frac{(\epsilon_\rho-\epsilon_{\phi,z})}{2}C_m^+C_n^{\dagger,+}J_{n-1}(\alpha_n r)J_{m+1}(\alpha_m r)+\frac{(\epsilon_\rho+\epsilon_{\phi,z})}{2}C_m^-C_n^{\dagger,+}J_{n-1}(\alpha_n r)J_{m-1}(\alpha_m r)\right] \\ &\quad\times e^{i(m-1)\phi}e^{-i(n-1)\phi} \end{aligned}$$

Finally, the last term of Eq. (77) is

$$E_n^{\dagger,z}E_m^z = C_n^EC_m^EJ_n(\alpha_n r)J_m(\alpha_m r)e^{-in\phi}e^{im\phi} \tag{78}$$

We integrate Eq. (77) over the cross-section of the cylinder.

{eq:intee}
$$\int\int \boldsymbol{E}_n^\dagger\cdot\Delta\bar{\bar{\epsilon}}\boldsymbol{E}_m = \int_0^a\int_0^{2\pi}(E_n^{\dagger,-}E_m^+ + E_n^{\dagger,+}E_m^- + E_n^{\dagger,z}E_m^z)r d\phi dr. \tag{79}$$

In Eq. (79), we separate the integrals over the r and θ. The angular integrals are nulls, excepts for $n=m$. Therefore, we can rewrite Eq. (79) as

{eq:inteedev}
$$\begin{aligned} \int\int \boldsymbol{E}_n^\dagger\cdot\Delta\bar{\bar{\epsilon}}\boldsymbol{E}_m &= \frac{(\epsilon_\rho-\epsilon_{\phi,z})}{2}C_m^-C_n^{\dagger,-}I_{n+1,m-1}(\alpha_m,\alpha_n,a)+\frac{(\epsilon_\rho+\epsilon_{\phi,z})}{2}C_m^+C_n^{\dagger,-}I_{n+1,m+1}(\alpha_m,\alpha_n,a) \\ &\quad+\frac{(\epsilon_\rho-\epsilon_{\phi,z})}{2}C_m^+C_n^{\dagger,+}I_{n-1,m+1}(\alpha_m,\alpha_n,a)+\frac{(\epsilon_\rho+\epsilon_{\phi,z})}{2}C_m^-C_n^{\dagger,+}I_{n-1,m-1}(\alpha_m,\alpha_n,a) \\ &\quad+\epsilon_{\phi,z}C_n^EC_m^EI_{m,m}(\alpha_m,\alpha_n,a) \end{aligned} \tag{80}$$

where $I_{n,m}(\alpha_1,\alpha_2,a) = 2\pi\int_0^a rJ_n(\alpha_1 r)J_m(\alpha_2 r)dr$.

E The incident plane wave

{sec:intincf}

We consider plane wave incident on the cylinder with along the direction $k=\beta\hat{\boldsymbol{z}}+\alpha\hat{\boldsymbol{x}}$. The electric field can be written as

$$\boldsymbol{E}_0 = (E_0^x\hat{\boldsymbol{x}}+E_0^y\hat{\boldsymbol{y}}+E_0^z\hat{\boldsymbol{z}})e^{i\beta z+i\alpha r\cos\phi}, \tag{81}$$

where $E_0^y=0$ for a $p-$polarization incident wave, and $E_0^x=E_0^z=0$ for a $s-$polarization. In the cylindrical base of vectors, it is rewritten as,

{eq:plwcyl}
$$\boldsymbol{E}_0 = \left[(E_0^x\cos\phi+E_0^y\sin\phi)\hat{\boldsymbol{e}}_\rho+(-E_0^x\sin\phi+E_0^y\cos\phi)\hat{\boldsymbol{e}}_\phi+E_0^z\hat{\boldsymbol{z}}\right]e^{i\beta z+i\alpha r\cos\phi}. \tag{82}$$

We multiply the incident field by the permittivity contrast $\Delta\bar{\bar{\epsilon}}$,

{eq:eplwcyl}
$$\Delta\bar{\bar{\epsilon}}\boldsymbol{E}_0 = \left[\epsilon_\rho(E_0^x\cos\phi+E_0^y\sin\phi)\hat{\boldsymbol{e}}_\rho+\epsilon_{\phi,z}(-E_0^x\sin(\theta)+E_0^y\cos\phi)\hat{\boldsymbol{e}}_\phi+\epsilon_{\phi,z}E_0^z\hat{\boldsymbol{z}}\right]e^{i\beta z+i\alpha r\cos\phi}. \tag{83}$$

Using the Jacobi-Anger expansion [51], to develop the solution into scalar cylindrical wave functions using J_m the Bessel function of first kind.

{Eq:Bessel_id}
$$e^{i\alpha r\cos(\phi)} = \sum_n i^nJ_n(\alpha r)e^{in\phi}. \tag{84}$$

So, each mode of the plane wave expansion becomes,

$$\begin{aligned}\Delta\bar{\bar{\epsilon}}E_0 &= \sum_m i^m J_m(\alpha r)\Big(\epsilon_\rho(E_0^x\cos\phi + E_0^y\sin\phi)\hat{\boldsymbol{e}}_\rho + \epsilon_{\phi,z}(-E_0^x\sin\phi + E_0^y\cos\phi)\hat{\boldsymbol{e}}_\phi + \epsilon_{\phi,z}E_0^z\hat{\boldsymbol{z}}\Big) \\ &\quad\times e^{im\phi}e^{i\beta z}\end{aligned} \tag{85}$$

Therefore, by writing it in the rotational base,

$$\begin{aligned}\Delta\bar{\bar{\epsilon}}E_0\cdot\hat{\boldsymbol{e}}_+ &= \frac{1}{2\sqrt{2}}\sum_m i^m J_m(\alpha r)(\epsilon_\rho - \epsilon_{\phi,z})(E_0^x - iE_0^y)e^{i(m+2)\phi}e^{i\beta z} \\ &\quad+\frac{1}{2\sqrt{2}}\sum_m i^m J_m(\alpha r)(\epsilon_{\phi,z} + \epsilon_\rho)(E_0^x + iE_0^y)e^{im\phi}e^{i\beta z}\end{aligned}$$

Similarly,

$$\begin{aligned}\Delta\bar{\bar{\epsilon}}E_0\cdot\hat{\boldsymbol{e}}_- &= \frac{1}{2\sqrt{2}}\sum_m i^m J_m(\alpha r)(\epsilon_{\phi,z} + \epsilon_\rho)(E_0^x - iE_0^y)e^{im\phi}e^{i\beta z} \\ &\quad+\frac{1}{2\sqrt{2}}\sum_m i^m J_m(\alpha r)(\epsilon_\rho - \epsilon_{\phi,z})(E_0^x + iE_0^y)e^{i(m-2)\phi}e^{i\beta z}\end{aligned}$$

So for each modes, we have to calculate the integral of product of $\boldsymbol{E}_n^\dagger$ by $\Delta\bar{\bar{\epsilon}}^b\boldsymbol{E}_0$

$$\begin{aligned}E_n^{\dagger,-}E_0^+ &= \frac{1}{2\sqrt{2}}C_n^{\dagger,-}(\epsilon_\rho - \epsilon_{\phi,z})(E_0^x - iE_0^y)\sum_m i^m J_{n+1}(\alpha_n r)J_m(\alpha r)e^{-i(n+1)\phi}e^{i(m+2)\phi} \\ &\quad+\frac{1}{2\sqrt{2}}C_{n'}^{\dagger,-}(\epsilon_{\phi,z} + \epsilon_\rho)(E_0^x + iE_0^y)\sum_m i^m J_{n+1}(\alpha_n r)J_m(\alpha r)e^{-i(n+1)\phi}e^{im\phi}\end{aligned}$$

The integral is then,

$$\begin{aligned}\int_0^a\int_0^{2\pi} E_n^{\dagger,-}E_0^+ r d\phi dr &= i^{n-1}C_n^{\dagger,-}\frac{\epsilon_\rho - \epsilon_\rho}{2}\frac{E_0^x - iE_0^y}{\sqrt{2}}I_{n+1,n-1}(\alpha_n,\alpha,a) \\ &\quad+i^{n+1}C_n^{\dagger,-}\frac{\epsilon_\rho + \epsilon_{\phi,z}}{2}\frac{E_0^x + iE_0^y}{\sqrt{2}}I_{n+1,n+1}(\alpha_n,\alpha,a)\end{aligned}$$

For the second term,

$$\begin{aligned}E_n^{\dagger,+}E_0^- &= \frac{1}{2\sqrt{2}}C_n^{\dagger,+}(\epsilon_{\phi,z} + \epsilon_\rho)(E_0^x - iE_0^y)\sum_m i^m J_{n-1}(\alpha_n r)J_m(\alpha r)e^{-i(n-1)\phi}e^{im\phi} \\ &\quad+\frac{1}{2\sqrt{2}}C_n^{\dagger,+}(\epsilon_\rho - \epsilon_{\phi,z})(E_0^x + iE_0^y)\sum_m i^m J_{n-1}(\alpha_n r)J_m(\alpha r)e^{-i(n-1)\phi}e^{i(m-2)\phi}\end{aligned}$$

The integral is then,

$$\begin{aligned}\int_0^a\int_0^{2\pi} E_n^{\dagger,+}E_0^- r d\phi dr &= i^{n-1}C_n^{\dagger,+}\frac{\epsilon_{\phi,z} + \epsilon_\rho}{2}\frac{E_0^x - iE_0^y}{\sqrt{2}}I_{n-1,n-1}(\alpha_n,\alpha,a) \\ &\quad+i^{n+1}C_n^{\dagger,+}\frac{\epsilon_\rho - \epsilon_{\phi,z}}{2}\frac{E_0^x + iE_0^y}{\sqrt{2}}I_{n-1,n+1}(\alpha_n,\alpha,a)\end{aligned}$$

For the last term, we have finally,

{eq:eplwcylsum}

$$\begin{aligned} E_n^{\dagger,z} E_0^z &= C_n^E J_n(\alpha_n r) e^{-in\phi} \sum_m i^m J_m(\alpha r) \epsilon_{\phi,z} E_0^z e^{im\phi} \\ &= C_n^E \epsilon_{\phi,z} E_0^z \sum_m i^m J_n(\alpha_n r) J_m(\alpha r) e^{-in\phi} e^{im\phi} \end{aligned} \tag{86}$$

The integral is then,

$$\int_0^a \int_0^{2\pi} E_n^{\dagger,z} E_0^z r d\theta dr = \epsilon_\rho i^n C_n^E E_0^z I_{n,n}(\alpha_n, \alpha, a) \tag{87}$$

References

[1] S. N. Samaddar, "Scattering of plane waves from an infinitely long cylinder of anisotropic materials at oblique incidence with an application to an electronic scanning antenna", Applied Scientific Research, Section B **10**, 385–411 (1962).

[2] R. Graglia and P. Uslenghi, "Electromagnetic scattering from anisotropic materials, part I: General theory", IEEE Transactions on Antennas and Propagation **32**, 867–869 (1984).

[3] R. D. Graglia, P. L. E. Uslenghi, and R. S. Zich, "Moment method with isoparametric elements for three-dimensional anisotropic scatterers", Proceedings of the IEEE **77**, 750–760 (1989).

[4] J. Monzon and N. Damaskos, "Two-dimensional scattering by a homogeneous anisotropic rod", IEEE Transactions on Antennas and Propagation **34**, 1243–1249 (1986).

[5] J. Monzon, "Three-dimensional scattering by an infinite homogeneous anisotropic circular cylinder: A spectral approach", IEEE Transactions on Antennas and Propagation **35**, 670–682 (1987).

[6] R.-B. Wu and C. H. Chen, "Variational Reaction Formulation of Scattering Problem for Anisotropic Dielectric Cylinders", IEEE Transactions on Antennas and Propagation **34**, 640–645 (1986).

[7] J. C. Monzon, "On a surface integral representation for homogeneous anisotropic regions: two-dimensional case", IEEE Transactions on Antennas and Propagation **36**, 1401–1406 (1988).

[8] B. Beker and K. Umashankar, "Analysis of Electromagnetic Scattering by Arbitrarily Shaped Two-Dimensional Anisotropic Objects: Combined Field Surface Integral Equation Formulation", Electromagnetics **9**, 215–229 (1989).

[9] N. Uzunoglu, P. Cottis, and J. Fikioris, "Excitation of electromagnetic waves in a gyroelectric cylinder", IEEE Transactions on Antennas and Propagation **33**, 90–99 (1985).

[10] V. V. Varadan, A. Lakhtakia, and V. K. Varadan, "Scattering by three-dimensional anisotropic scatterers", IEEE Transactions on Antennas and Propagation **37**, 800–802 (1989).

[11] C. M. Rappaport and E. B. Smith, "Anisotropic FDFD computed on conformal meshes", IEEE Transactions on Magnetics **27**, 3848–3851 (1991).

[12] Weimin Sun and C. A. Balanis, "Edge-based FEM solution of scattering from inhomogeneous and anisotropic objects", IEEE Transactions on Antennas and Propagation **42**, 627–632 (1994).

[13] X. B. Wu and K. Yasumoto, "Three-dimensional scattering by an infinite homogeneous anisotropic circular cylinder: An analytical solution", Journal of Applied Physics **82**, 1996–2003 (1997).

[14] W. Ren, "Contributions to the electromagnetic wave theory of bounded homogeneous anisotropic media", Physical Review E **47**, 664–673 (1993).

[15] R. Sammut and A. W. Snyder, "Leaky modes on a dielectric waveguide: orthogonality and excitation", Applied Optics **15**, 1040–1044 (1976).

[16] E. A. Muljarov, W. Langbein, and R. Zimmermann, "Brillouin-Wigner perturbation theory in open electromagnetic systems", EPL (Europhysics Letters) **92**, 50010 (2010).

[17] R. Colom, R. McPhedran, B. Stout, and N. Bonod, "Modal expansion of the scattered field: Causality, nondivergence, and nonresonant contribution", Physical Review B **98**, 085418 (2018).

[18] E. A. Muljarov and T. Weiss, "Resonant-state expansion for open optical systems: generalization to magnetic, chiral, and bi-anisotropic materials", Optics Letters **43**, 1978–1981 (2018).

[19] P. Y. Chen, D. J. Bergman, and Y. Sivan, "Generalizing Normal Mode Expansion of Electromagnetic Green's Tensor to Open Systems", Physical Review Applied **11**, 044018 (2019).

[20] C. Forestiere, G. Gravina, G. Miano, M. Pascale, and R. Tricarico, "Electromagnetic modes and resonances of two-dimensional bodies", Physical Review B **99**, 155423 (2019).

[21] P. Y. Chen, Y. Sivan, and E. A. Muljarov, "An efficient solver for the generalized normal modes of non-uniform open optical resonators", (2020).

[22] D. J. Bergman and D. Stroud, "Theory of resonances in the electromagnetic scattering by macroscopic bodies", Physical Review B **22**, 3527–3539 (1980).

[23] A. Farhi and D. J. Bergman, "Electromagnetic eigenstates and the field of an oscillating point electric dipole in a flat-slab composite structure", Physical Review A **93**, 063844 (2016).

[24] C. Forestiere and G. Miano, "Material-independent modes for electromagnetic scattering", Physical Review B **94**, 201406 (2016).

[25] M. Pascale, G. Miano, and C. Forestiere, "Spectral theory of electromagnetic scattering by a coated sphere", JOSA B **34**, 1524–1535 (2017).

[26] P. Y. Chen and Y. Sivan, "Robust Location of Optical Fiber Modes via the Argument Principle Method", Computer Physics Communications **214**, 105–116 (2017).

[27] C. Forestiere, G. Miano, G. Rubinacci, A. Tamburrino, R. Tricarico, and S. Ventre, "Volume Integral Formulation for the Calculation of Material Independent Modes of Dielectric Scatterers", IEEE Transactions on Antennas and Propagation **66**, 2505–2514 (2018).

[28] M. Pascale, G. Miano, R. Tricarico, and C. Forestiere, "Full-wave electromagnetic modes and hybridization in nanoparticle dimers", Scientific Reports **9**, 1–21 (2019).

[29] G. Rosolen, P. Y. Chen, B. Maes, and Y. Sivan, "Overcoming the bottleneck for quantum computations of complex nanophotonic structures: Purcell and FRET calculations using a rigorous mode hybridization method", (2019).

[30] N. Maccaferri, Y. Zhao, T. Isoniemi, M. Iarossi, A. Parracino, G. Strangi, and F. De Angelis, "Hyperbolic Meta-Antennas Enable Full Control of Scattering and Absorption of Light", Nano Letters (2019).

[31] X. Yang, J. Yao, J. Rho, X. Yin, and X. Zhang, "Experimental realization of three-dimensional indefinite cavities at the nanoscale with anomalous scaling laws", Nature Photonics **6**, 450–454 (2012).

[32] J. Yao, X. Yang, X. Yin, G. Bartal, and X. Zhang, "Three-dimensional nanometer-scale optical cavities of indefinite medium", Proceedings of the National Academy of Sciences **108**, 11327–11331 (2011).

[33] X. Yin, H. Zhu, H. Guo, M. Deng, T. Xu, Z. Gong, X. Li, Z. H. Hang, C. Wu, H. Li, S. Chen, L. Zhou, and L. Chen, "Hyperbolic Metamaterial Devices for Wavefront Manipulation", Laser & Photonics Reviews **13**, 1800081 (2019).

[34] D. Lu, J. J. Kan, E. E. Fullerton, and Z. Liu, "Enhancing spontaneous emission rates of molecules using nanopatterned multilayer hyperbolic metamaterials", Nature Nanotechnology **9**, 48–53 (2014).

[35] S. Molesky, C. J. Dewalt, and Z. Jacob, "High temperature epsilon-near-zero and epsilon-near-pole metamaterial emitters for thermophotovoltaics", 15 (2012).

[36] R. Kumar and K. Kajikawa, "Superscattering from cylindrical hyperbolic metamaterials in the visible region", Optics Express **28**, 1507–1517 (2020).

[37] C. D.-A. Nó, M. Naserpour, and C. J. Zapata-Rodríguez, "Tunable Scattering Cancellation of Light Using Anisotropic Cylindrical Cavities", Plasmonics **12**, 675–683 (2017).

[38] Z. Guo, H. Jiang, and H. Chen, "Hyperbolic metamaterials: From dispersion manipulation to applications", Journal of Applied Physics **127**, 071101 (2020).

[39] A. Poddubny, I. Iorsh, P. Belov, and Y. Kivshar, "Hyperbolic metamaterials", Nature Photonics **7**, 948–957 (2013).

[40] A. D. Rakić, A. B. Djurišić, J. M. Elazar, and M. L. Majewski, "Optical properties of metallic films for vertical-cavity optoelectronic devices", Applied Optics **37**, 5271–5283 (1998).

[41] T. Siefke, S. Kroker, K. Pfeiffer, O. Puffky, K. Dietrich, D. Franta, I. Ohlídal, A. Szeghalmi, E.-B. Kley, and A. Tünnermann, "Materials Pushing the Application Limits of Wire Grid Polarizers further into the Deep Ultraviolet Spectral Range", Advanced Optical Materials **4**, 1780–1786 (2016).

[42] P. Shekhar, J. Atkinson, and Z. Jacob, "Hyperbolic metamaterials: fundamentals and applications", Nano Convergence **1**, 14 (2014).

[43] T. C. Choy, *Effective Medium Theory: Principles and Applications* (Oxford University Press, Dec. 17, 2015), 257 pp.

[44] P. Y. Chen, D. J. Bergman, and Y. Sivan, "Spectral decomposition of the Lippmann-Schwinger equation applied to cylinders", (2017).

[45] H. Kettunen, H. Wallén, and A. Sihvola, "Tailoring Effective Media by Mie Resonances of Radially-Anisotropic Cylinders", Photonics **2**, 509–526 (2015).

[46] H. L. Chen and L. Gao, "Anomalous electromagnetic scattering from radially anisotropic nanowires", Physical Review A **86**, 033825 (2012).

[47] A. I. Kuznetsov, A. E. Miroshnichenko, M. L. Brongersma, Y. S. Kivshar, and B. Luk'yanchuk, "Optically resonant dielectric nanostructures", Science **354**, aag2472 (2016).

[48] M. Kerker, D.-S. Wang, and C. L. Giles, "Electromagnetic scattering by magnetic spheres", Journal of the Optical Society of America **73**, 765 (1983).

[49] W. Liu and Y. S. Kivshar, "Generalized Kerker effects in nanophotonics and meta-optics [Invited]", Optics Express **26**, 13085 (2018).

[50] P. D. Terekhov, K. V. Baryshnikova, Y. A. Artemyev, A. Karabchevsky, A. S. Shalin, and A. B. Evlyukhin, "Multipolar response of nonspherical silicon nanoparticles in the visible and near-infrared spectral ranges", Physical Review B **96**, 035443 (2017).

[51] M. Born and E. Wolf, *Principle of Optics*, 7th ed. (Cambridge, 1999).

[52] P. Tsao, "Derivation and implications of the symmetry property of the permittivity tensor", American Journal of Physics **61**, 823–825 (1993).

[53] Y. Kantor and D. J. Bergman, "Elastostatic resonances—a new approach to the calculation of the effective elastic constants of composites", Journal of the Mechanics and Physics of Solids **30**, 355–376 (1982).

[54] M. I. Stockman, "Spaser Action, Loss Compensation, and Stability in Plasmonic Systems with Gain", Physical Review Letters **106** (2011).

[55] S. Höfer, J. Popp, and T. G. Mayerhöfer, "Determination of the dielectric tensor function of triclinic CuSO4·5H2O", Vibrational Spectroscopy **67**, 44–54 (2013).

[56] Y. E, J. Yao, and L. Wang, "Propagation of terahertz waves in a monoclinic crystal BaGa4Se7", Scientific Reports **8**, 16229 (2018).

[57] Jin Au Kong, "Theorems of bianisotropic media", Proceedings of the IEEE **60**, 1036–1046 (1972).

[58] A. Villeneuve and R. Harrington, "Reciprocity Relationships for Gyrotropic Media", IRE Transactions on Microwave Theory and Techniques **6**, 308–310 (1958).

[59] P. S. Pershan, "Magneto-Optical Effects", Journal of Applied Physics **38**, 1482–1490 (1967).